Natural Hazards
https://doi.org/10.1007/s11069-025-07548-x

ORIGINAL PAPER

Seasonal outlooks for coastal high-tide flooding

Ryan Holmes[1] · **Océane Richet**[1] · **Ben Hague**[1] · **Grant Smith**[1] · **Claire Spillman**[1]

Received: 19 January 2025 / Accepted: 20 July 2025

Abstract
Chronic "high-tide" flooding is a growing concern for coastal communities in Australia and globally as sea levels rise. Early warnings of such events can help coastal managers prepare for their impacts. Building on previous work, we construct predictions of daily coastal sea level and threshold exceedance probability that provide information on high-tide flooding risks over the coming season/s. Our trial forecast system combines tide predictions and relative sea level rise projections with statistical representations of storm surges and ensemble monthly-mean sea level anomaly predictions from a dynamical seasonal forecast model. We assess the system's performance at tide gauges around the Australian coastline and in the western Pacific islands. The system out-performs tide-only and climatological reference forecasts for daily maximum sea level at all locations, and beats a best constant reference forecast for 99th percentile threshold exceedance probability at most locations. Including seasonal sea level anomaly predictions from the dynamical model improves performance by up to $\sim$ 20% in north-west Australia and $\sim$ 40% in the Pacific islands, decreasing with lead time. Introducing a reliability calibration significantly improves threshold exceedance forecast skill at locations with complex tidal dynamics where harmonic tide predictions struggle to capture the highest high tides. We show that forecast skill is sensitive to the choice of impact-based (e.g., minor) or likelihood-based (e.g., 99th percentile) flood threshold, highlighting the importance of defining locally-relevant thresholds for application of the warning system. The development of real-time forecast guidance products to suit a range of potential stakeholders, from emergency services and meteorological agencies to coastal and ecosystem managers and port authorities, is ongoing.

Keywords Coastal flooding · Seasonal prediction · Forecast verification · Sea level rise

1 Introduction

The frequency and severity of coastal flooding events are increasing across the globe, and are expected to increase further with sea level rise (McInnes et al. 2016; Cooley et al. 2022). The potential for serious future impacts in the Australian region has been recognized through the classification of coastal flooding as a priority hazard in

✉ Ryan Holmes
ryan.holmes@bom.gov.au

[1] Bureau of Meteorology, Sydney, Australia

Australia's first National Climate Risk Assessment (Department of Climate Change 2024). Extreme events associated with, for example, tropical cyclone storm surges (Needham et al. 2015; Mortlock et al. 2018) and other short-lived atmospheric phenomena such as East Coast Lows (Callaghan and Power 2014) are important due to their acute impacts on property, infrastructure and loss of life. In contrast, regular minor or nuisance flooding (e.g. due to tides alone) can have chronic and cumulative impacts on communities through, for example, road and sidewalk closures, saltwater intrusions and blocked storm drainage and waste water treatment systems with their associated public health impacts (e.g. Flood and Cahoon 2011; Hanslow et al. 2018; Hino et al. 2019; Kasmalkar et al. 2020; Hauer et al. 2021; Allison et al. 2024). There is evidence that the cost of these regular minor events may become comparable to that of extreme events in some locations due to their cumulative impacts (Moftakhari et al. 2017; Paulik et al. 2021). The increasing observed (e.g. Sweet 2018; Hague et al. 2020, 2022) and projected (Sweet and Park 2014; Vandenberg-Rodes et al. 2016; Thompson et al. 2021; Hague et al. 2024) frequency and impacts on coastal communities of such "high-tide flooding" events, so-named because they are often associated with king tides and the lack of a specific meteorological driver, requires such communities to consider adaptation measures (Ayşın Dedekorkut-Howes et al. 2021; Mortensen et al. 2024). For adaptation to be effective, quantitative knowledge of the risk and how it may change in the future is critical.

Seasonal outlooks of expected coastal sea level variability over the next 1 to 12 months, particularly of high-tide flooding risk, can inform decision making and risk management by coastal managers and stakeholders. Decisions that could be informed by skillful seasonal outlooks include hazard planning for coastal infrastructure (e.g. ports, roads, buildings), scheduling for coastal activities, access and maintenance, and workforce planning for emergency services and meteorological agencies. Skillful seasonal coastal sea level predictions can also inform environmental management decision-making and planning. Sea level extremes can impact coastal ecosystems through processes ranging from salt-water intrusions and coastal erosion under high-water events to coral reef exposure and mangrove diebacks during "low-water droughts" (e.g. Brown et al. 2019; Ampou et al. 2017; Abhik et al. 2021; Widlansky et al. 2014). Loss of access to sites and poor outcomes for conservation efforts can also result from sea level extremes. Many of these decisions are already being informed by information from conventional tide tables (as well as storm-tide forecasts at numerical weather prediction lead times). However, the potential added decision-making value of full-feature seasonal sea level outlooks, that also include forecast information on non-tidal sea level variability, has not been explored in detail. Recent advances in seasonal forecasting of non-tidal sea level variability (e.g. Widlansky et al. 2017; McIntosh et al. 2015; Long et al. 2021; Holmes et al. 2025) suggest that such a system, combining seasonal forecasts of non-tidal residuals with tide predictions and other climatological information, may now be possible. This is what we explore in this study.

Here we present seasonal sea level and high-tide flooding outlooks which combine forecast information for a number of different contributions to sea level variability that are skillful on daily time scales from 1 to 12 months into the future. This trial forecast system builds on the work of Dusek et al. (2022) and Stephens et al. (2014). Dusek et al. (2022) developed a probabilistic system for forecasting daily high-tide flooding risk at tide gauges around the North American coastline and Pacific islands. They did this by combining deterministic tide predictions and sea level rise projections with probabilistic, climatological distributions of the non-tidal residuals (defined

as the observed sea level minus the tide prediction and sea level rise). These non-tidal residuals include the effects of storm surges, atmospheric pressure variations, waves and other processes observed at a tide gauge that, while not directly predictable beyond a typical weather forecast time-scale, have a seasonality that can be incorporated into the forecast system based on past observations. Dusek et al. (2022) showed that their system was more skillful than a constant reference forecast (corresponding to the observed past frequency of events) at the majority of the US east, west and Pacific island locations they considered for the specific set of impact-based minor-flooding thresholds they considered.

A variety of subseasonal to seasonal (and beyond) processes, associated with modes of climate variability such as the El Niño-Southern Oscillation (ENSO) and the Interdecadal Pacific Oscillation (IPO), also contribute to sea level variability (Frankcombe et al. 2015; Woodworth et al. 2019) and are known to modulate coastal flooding frequencies and impact ecosystems in some locations (e.g. Widlansky et al. 2014; Muis et al. 2018; Lowe et al. 2021; Sweet et al. 2024). These processes act in addition to the sea level seasonal cycle, which in this study is captured within the tidal prediction by the annual and semi-annual tidal constituents (Parker (2007); Ray and Merrifield (2019), see Sect. 2 and Appendix A for more discussion of how long period tidal constituents are treated) and residual climatological distributions. A number of recent studies have shown that some seasonal sea level anomalies are predictable out to and beyond 6 months into the future using current-generation dynamical seasonal forecast systems (e.g. Widlansky et al. 2017; McIntosh et al. 2015; Long et al. 2021; Holmes et al. 2025). In an extension to their climatological forecast system, Dusek et al. (2022) showed that including a simple persistence-based seasonal forecast, where the sea level anomaly from the previous month is assumed to persist into the future, led to improvements in forecast skill along the US west coast and in the Pacific islands where persistence is significant due to the influence of ENSO. This option was also explored by Stephens et al. (2014), who combined tide predictions with forecasts of low-frequency mean sea level variability to construct high-water alerts for the Pacific islands.

In this article, we develop a trial Seasonal Outlooks for High Tide Flooding (SOHTF) forecast system that provides probabilistic information on daily coastal sea level 1–12 months into the future. SOHTF is based on the work of Dusek et al. (2022) and combines tide predictions and sea level rise projections with climatological distributions of the non-tidal residual from tide gauge observations (see Sect. 2). Our work advances upon Dusek et al. (2022) by (1) assessing the skill of a similar system applied to tide gauges in the Australian and western Pacific region (Fig. 1a), (2) verifying the probabilistic raw sea level forecasts (using the continuous ranked probability score, CRPS) in addition to high-tide flooding threshold exceedance probability forecasts (Sect. 3), (3) including dynamical seasonal sea level forecasts from the Bureau of Meterology's seasonal forecast system, ACCESS-S2 (Wedd et al. 2022; Holmes et al. 2025, Sect. 4) (4) exploring a number of additional advancements including a reliability calibration step (Sect. 5 and Appendix A) and (5) quantifying the sensitivity of threshold exceedance forecast skill to different choices of impact-based and likelihood-based flood thresholds (Sect. 6). In Sect. 6 we also briefly consider low-water extremes, given the potential for forecast applications related to shipping, port access and ecosystem impacts. We conclude with a summary of our results, a discussion of the potential applications of SOHTF as well as future work (Sect. 7).

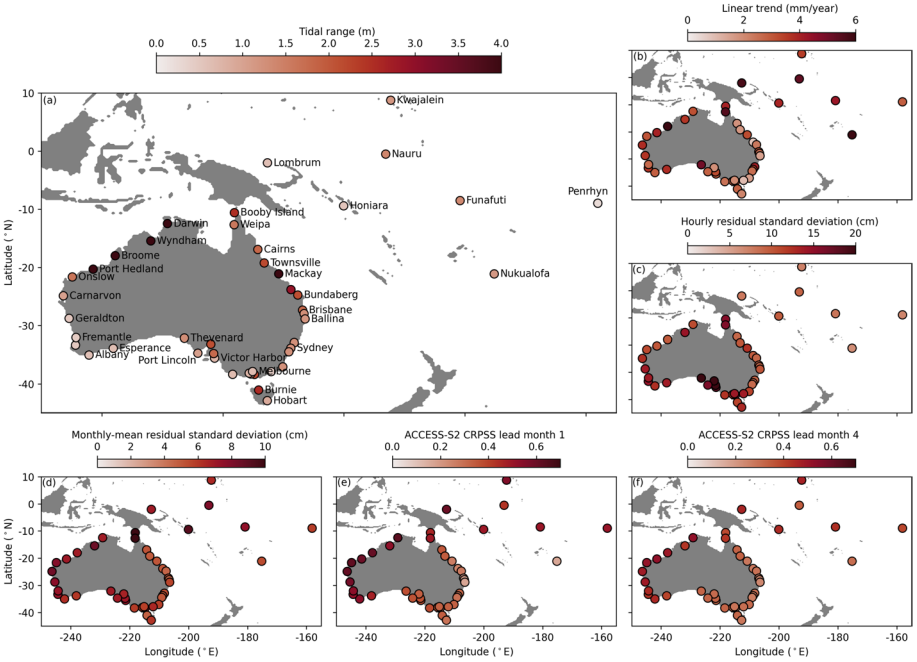

Fig. 1 **a** Tidal range (defined as the mean daily high tide minus the mean daily low tide), **b** linear trend, **c** non-tidal residual standard deviation, **d** monthly-mean residual standard deviation and ACCESS-S2 monthly-mean anomaly CRPS skill score (relative to a climatological forecast, see methods) at lead months **e** 1 and **f** 4 for each tide gauge location considered in this study. The time period considered for these metrics is 1982–2018 for the ANCHORS locations (coastal Australia) and 1993–2018 for the UHSLC locations (Pacific islands)

2 Methods

2.1 Data

We use hourly observations of total water level, $\eta_o(t)$, from the Australian National Collection of Homogenized Observations of Relative Sea Level (ANCHORS) tide gauge dataset (Hague et al. 2022). In addition to the ANCHORS data, we also include several western Pacific island tide gauges (from the University of Hawaii Sea Level Center, UHSLC, Caldwell et al. (2001), https://uhslc.soest.hawaii.edu/data/) in order to provide a contrast with the Australian locations given the differing coastal sea level dynamics around islands compared to the Australian continent, and the increased seasonal predictability in the tropical Pacific region (e.g. Widlansky et al. 2017). These western Pacific locations, indicated in Fig. 1a, were chosen to represent a range of latitudes, tidal ranges, and seasonal predictability (SOHTF forecast skill had no influence on this choice of stations). Our analysis is based on observations over the periods 1982–2018 (for the ANCHORS gauges) and 1993–2018 (for the UHSLC gauges), referred to as the hindcast period.

2.2 Probabilistic total sea level forecasts

The SOHTF system combines four different components of sea level variability:

1. Astronomical tide predictions,
2. Sea level rise (long-term trend),
3. Climatological statistics of storm surges and high frequency variability,
4. Seasonal sea level anomalies from ACCESS-S2 ensemble predictions.

Based on these components, our prediction for the sea level at a given tide gauge can be written,

$$\begin{aligned}\eta_f(t) = &\ \eta_{\text{tide}}(t) \\ &+ \eta_{\text{SLR}}(t) \\ &+ \underbrace{\mathcal{N}\big(\mu_R(t_T, t_M), \sigma_R^2(i, t_T, t_M)\big)}_{\eta_{\text{res}}} \\ &+ i\ \underbrace{\mathcal{N}\big(\mu_S(t), \sigma_S^2(t)\big)}_{\eta_{\text{seasonal}}},\end{aligned} \tag{1}$$

where t is time with hourly resolution and each line in the equation represents the equivalent component (1–4) above of the sea level variability. $\eta_{\text{tide}}(t)$ and $\eta_{\text{SLR}}(t)$ are treated deterministically, while $\eta_{\text{res}}(t)$ and $\eta_{\text{seasonal}}(t)$ are treated probabilistically through representation as Gaussian distributions, $\mathcal{N}(\mu, \sigma^2)$, characterized by their mean, μ and standard deviation, σ. Each component is described in more detail in the following subsections. We will mainly focus on two versions of the system:

- SOHTF-CLIM: This version, corresponding to setting $i = 0$ in Eq. (1), does not include ACCESS-S2 predictions and is thus roughly equivalent to the climatological system proposed by Dusek et al. (2022) (with differences noted below).
- SOHTF-S2: This version, corresponding to setting $i = 1$ in Eq. (1), does include ACCESS-S2 predictions, with a modification to the residual variance (third line in Eq. (1)) to avoid double counting the seasonal variability as described in more detail below.

2.2.1 Tide predictions (deterministic)

Our tide predictions [η_{tide} in Eq. (1)] are based on harmonic analysis of the tide gauge data over the full hindcast period using the Utide software package (https://pypi.org/project/UTide/, Codiga (2011)). We use a set of 146 tidal constituents which includes all the major diurnal and semi-diurnal constituents as well as shallow water constituents and the annual and semi-annual constituents, *Sa* and *Ssa*. Therefore, the tide component of the forecast captures the seasonal cycle of mean sea level, characterized by higher maximum tide heights along the south coast in winter and in the north in summer (Fig. 2a), as well as the long-term 4.4 and 18.6-year nodal cycles (Haigh et al. 2011; Enríquez et al. 2022). No trend term is included in the tide prediction and no data filling is performed prior to the prediction. These choices are based on a sensitivity analysis performed using a variety of tide prediction configurations, as discussed in more detail in Appendix A and in Richet et al. (2024). Note that the climatology calculations for the ACCESS-S2 component

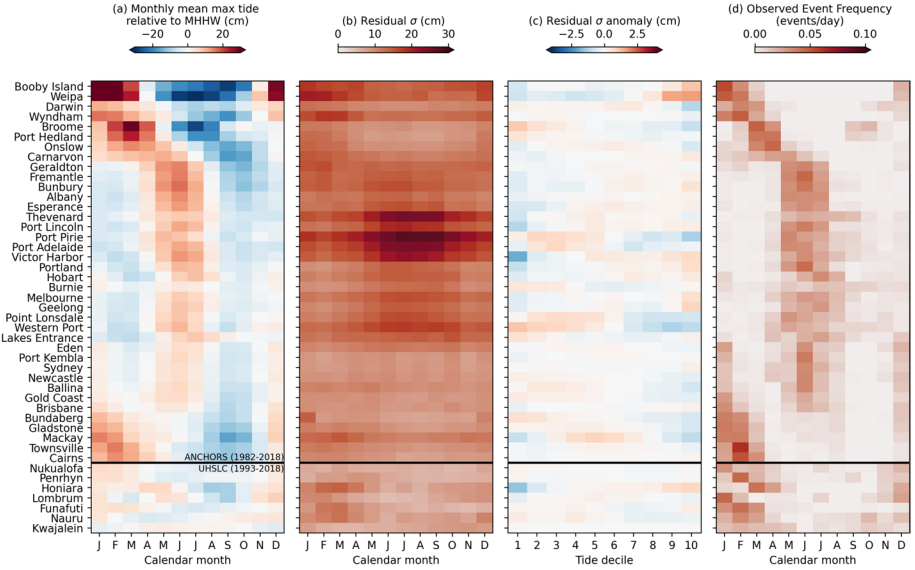

Fig. 2 Climatological statistics over the 1982–2018 (ANCHORS gauges) and 1993–2018 (UHSLC gauges) hindcast periods used in SOHTF. Australian tide gauges are listed in anti-clockwise order from top to bottom, with the western Pacific island gauges listed at the bottom below the black line. **a** Maximum tide height, relative to Mean Higher High Water (MHHW, the mean daily maximum tide over the hindcast period) by calendar month. **b** Climatology of non-tidal residual standard deviation by calendar month. **c** Residual standard deviation anomaly classed by tide decile. **d** Climatological frequency of high-tide flooding events (defined as exceedances of the 99th percentile of daily maximum total sea level) over the hindcast period

[η_{seasonal} in Eq. (1)] requires care to avoid double counting the seasonal cycle, as discussed in Sect. 2.2.4.

2.2.2 Sea level rise (deterministic)

We use the long-term trend in sea level, based on either a quadratic or a linear fit to the total hourly sea level over the hindcast period, as a deterministic component of the forecast [η_{SLR} in Eq. (1)]. No data filling is performed prior to computing these trends. We do not consider the role of vertical land motion in this study. For the Australian tide gauges, we use a quadratic rather than linear fit in order to capture acceleration in the rate of sea level rise (e.g. Hamlington et al. (2024)). However, for the western Pacific island tide gauges, where the hindcast period is shorter, we found that a linear fit was more robust (i.e. less influenced by climate variability, see Appendix A for a discussion of other possible approaches to the treatment of trends).

2.2.3 Residual statistics (probabilistic)

Following Dusek et al. (2022), we represent the non-tidal variability in the sea level using a set of climatological distributions of the residuals (the observed total sea level minus the

tide and trend computed as above) at each tide gauge location [η_{res} in Eq. (1)]. These distributions capture all processes that contribute to the observed variability at each gauge, such as storm surges, inverse barometer, coastal trapped waves, wave setup etc, and thus SOHTF constitutes a forecast of the total water level (although note that processes acting on timescales shorter than one hour are not properly represented in the underlying dataset). These distributions are assumed to be Gaussian with means and standard deviations, $\mu_R(t_M, t_T)$, $\sigma_R^2(i, t_M, t_T)$ that are computed from the hindcast period separately for each month of the year, $t_M(t) \in [1, 12]$. As discussed in Dusek et al. (2022), we make a Gaussian approximation for the residual distributions as we are focused on predicting relatively frequent events that occur within the bulk of the residual distribution where the normal assumption is a good approximation, rather than events at the tails (e.g. beyond 5%) associated with extreme storm surges. These distributions are then added to the deterministic tide and trend predictions to create a probabilistic forecast of total sea level for each month of the year that accounts for the observed seasonality in residual variability (Fig. 2b). For example, SOHTF captures the intensification of storm surge activity in the winter months along the south coast of Australia (most evident between Thevenard and Victor Harbor in Fig. 2b). In this way, our approach accounts for the seasonal dependence of storm surge and tide height maximums similar to the joint probability method used by Palmer et al. (2024). Note that in SOHTF-S2, when ACCESS-S2 predictions are included, the climatological distribution variance includes only high-frequency (submonthly) variability.

In addition to a dependence on the month of the year, the residual distributions are also dependent on deciles of the tide, $t_T(t) \in [1, 10]$, as an attempt to account for tide-residual interactions [following Dusek et al. (2022)]. This dependence is computed by binning the residuals by tide decile and computing the mean and standard deviation of the residuals in each bin. For the standard deviation, this is shown as an anomaly relative to the mean across all tidal deciles in Fig. 2c. The dependence is relatively weak in most locations, reaching 2.5cm in the most extreme cases.

2.2.4 Seasonal sea level anomalies (probabilistic)

We also explore the benefit of including seasonal sea level anomaly predictions [η_{seasonal} in Eq. (1)] taken from the Bureau of Meteorology's dynamical seasonal forecast model, ACCESS-S2 (Hudson et al. 2017; Wedd et al. 2022). ACCESS-S2's sea level predictions, described in more detail in Holmes et al. (2025), consist of a 27 member lagged-time ensemble of forecasts of monthly-mean sea level anomalies (including the inverse barometer effect added as a post-processing step) at 0.25° resolution globally, initialized at the beginning of every month over the hindcast period 1982–2018. ACCESS-S2 also provides real-time forecasts that are not discussed here. These forecasts are interpolated using nearest neighbour interpolation to each tide gauge location. The ACCESS-S2 sea level predictions are most skilful in the Pacific islands and the north and west coasts of Australia (Fig. 1e, f), with little skill on the south and east coasts beyond the first lead month (see Holmes et al. (2025) for more details).

Monthly mean ACCESS-S2 seasonal sea level anomalies are computed using a lead time-dependent climatology and long-term trend that matches the hindcast period used for the tide prediction, long-term trend and residual distribution computations described above. This matching of ACCESS-S2 climatology and tide analysis periods avoids double counting of variability captured by the tide predictions (e.g. radiational tides and the seasonal cycle). When used in SOHTF-S2, the ACCESS-S2 seasonal sea level anomalies are

added to the other forecast components using a normal distribution (chosen for simplicity) with ensemble mean and ensemble standard deviations computed across the 27 member ACCESS-S2 ensemble forecast at each lead time. Again, to avoid double counting, the climatological residual distributions are computed using only submonthly residuals (i.e. the monthly-mean is removed) when ACCESS-S2 is included, as denoted by the i dependence of σ_R^2 in Eq. (1).

For comparison purposes, we also consider a deterministic damped persistence seasonal forecast (as discussed in Dusek et al. (2022), denoted by SOHTF-Damped Persistence), computed by persisting forward the previous month's monthly-mean total sea level anomaly, multiplied by the autocorrelation of the monthly-mean total sea level anomaly over the hindcast period (see Sect. 4).

2.3 Threshold exceedance forecasts

In addition to the probabilistic total sea level forecast described by Eq. (1), SOHTF also includes forecasts of the probability of exceeding certain thresholds, η_{th}. For a given threshold η_{th}, these probabilities are computed as the area under the probabilistic total sea level prediction distribution that exceeds η_{th},

$$p_{\text{hourly}}(\eta > \eta_{th}) = 1 - F_f(\eta_{th}, t), \tag{2}$$

where $F_f(\eta, t) = \frac{1}{2}\left[1 + \text{erf}\left(\frac{\eta-\mu}{\sigma\sqrt{2}}\right)\right]$ is the cumulative distribution function corresponding to the predicted distribution η_f [i.e. from Eq. (1) a normal distribution with mean $\eta_{\text{tide}} + \eta_{\text{SLR}} + \mu_R + i\mu_S$ and standard deviation $\sqrt{\sigma_R^2 + i\sigma_S^2}$]. Following Dusek et al. (2022), we also compute daily probabilities of thresholds exceedance, $p_{\text{daily}}(\eta > \eta_{th})$, taking into account the auto-correlation of the hourly residuals via,

$$p_{\text{daily}} = p_{\max} + \sum_{t=1}^{23} \left[p_{\text{hourly}}(t)(1 - r(t))\right], \tag{3}$$

where $p_{\max}$ is the maximum hourly threshold exceedance probability within each day and $r(t)$ is the auto-correlation function of the hourly residuals (computed from the hindcast period) at lag t in hours from the hour of $p_{\max}$.

A critical consideration is the choice of threshold η_{th}. As impact-based high-tide flooding thresholds are not available for many of the locations we consider, we have instead used the 99th percentile of the daily maximum total sea level over the hindcast period. Such a threshold, corresponding to a frequency-based flooding definition of 3–4 events per year over the hindcast period on average, has been used in the past as a representative threshold for high-tide flooding events (e.g. Hague et al. 2022). However, in Sect. 6 we explore the sensitivity of our results to the choice of threshold, considering impact-based minor flooding thresholds from Hague et al. (2022) at locations where they are available, as well as considering more extreme likelihood-based thresholds to understand how forecast skill decays when considering more extreme events. In Sect. 6 we also consider low-water level thresholds [obtained by replacing $\eta > \eta_{th}$ in Eq. (2) with $\eta < \eta_{th}$] to understand the skill of the system at predicting low-water level extremes.

2.4 Skill metrics

The skill of SOHTF's total sea level prediction, η_f, is assessed using the continuous ranked probability score (CRPS), while threshold exceedance probability prediction skill is assessed using the Brier score (BS). Note that the CRPS can be interpreted as an integral of the BS for threshold exceedance probability forecasts averaged over all possible thresholds (Hersbach 2000), while the BS quantifies SOHTF's skill at predicting specifically the highest sea levels. Both the CRPS and BS are proper scores, in the sense that forecast distributions that are closest to the true observational distribution give optimum expected scores (Gneiting and Katzfuss 2014).

2.4.1 Continuous ranked probability score

The CRPS is defined as,

$$\mathrm{CRPS}(F_f, \eta_o) = \int_{-\infty}^{\infty} \left[F_f(\eta) - H(\eta - \eta_o)\right]^2 d\eta, \tag{4}$$

where F_f is the forecast cumulative distribution function, H is the heaviside step function (which takes the value 0 when the argument is negative and 1 otherwise) and η_o is the observed sea level. If η_f is deterministic, corresponding to a forecast distribution $F_f(\eta) = H(\eta - \eta_f)$, the CRPS reduces to the mean absolute error. Otherwise, tighter forecast distributions around the observed value η_o yield smaller, better CRPS scores. We convert CRPS to a skill score CRPSS,

$$\mathrm{CRPSS} = 1 - \frac{\mathrm{CRPS}}{\mathrm{CRPS}^{\mathrm{ref}}}, \tag{5}$$

where values of CRPSS greater than 0 indicate that the forecast has better CRPS than the CRPS of a reference forecast, $\mathrm{CRPS}^{\mathrm{ref}}$. In most cases we consider the climatological distribution of η_o at the given location from the given target month as our reference forecast, although we also consider several other reference forecasts (such as a tide-only deterministic forecast) in specific cases. As our probabilistic forecasts are always Gaussian distributions, the CRPS can be computed analytically as (Gneiting et al. 2005),

$$\mathrm{CRPS}(\mathcal{N}(\mu, \sigma^2), \eta_o) = \sigma \left\{ \frac{\eta_o - \mu}{\sigma} \left[2\Phi\left(\frac{\eta_o - \mu}{\sigma}\right) - 1 \right] + 2\phi\left(\frac{\eta_o - \mu}{\sigma}\right) - \frac{1}{\sqrt{\pi}} \right\}, \tag{6}$$

where $\phi(\frac{\eta_o - \mu}{\sigma})$ and $\Phi(\frac{\eta_o - \mu}{\sigma})$ denote the probability density and cumulative distribution functions of a normal distribution with mean 0 and standard deviation 1 respectively. Note that the CRPS verification can be performed across all months together, or separately as a function of calendar month in order to evaluate the seasonal dependence of forecast skill.

2.4.2 Brier score

Verification for SOHTF's threshold exceedance forecasts is based on the BS, the squared error in probability space,

$$\mathrm{BS} = \overline{(p - p^o)^2}, \tag{7}$$

where p is the probability forecast and p^o is the binary event time series, equal to 1 if the observed sea level exceeds the threshold and 0 otherwise. The overline indicates an average over all forecast cases (note that since our sea level thresholds are absolute, we only consider BS verification computed across all calendar months together). As for the CRPS [Eq. (5)], we compute a Brier skill score (BSS) by comparing the BS against $\mathrm{BS}^{\mathrm{ref}}$, the BS achieved by a reference forecast. We consider two reference forecasts; 1) the "best constant" reference forecast, which has a constant value of p corresponding to the observed frequency of threshold exceedances across all calendar months in the hindcast period at each location and 2) a "climatological" reference forecast, where p corresponds to the observed frequency of threshold exceedance only within the given calendar month (i.e. capturing the seasonal cycle of threshold exceedances).

2.4.3 CORP decomposition and reliability calibration

Finally, to better understand the threshold exceedance skill, and to perform a robust reliability calibration (see Sect. 5), we perform a Consistent, Optimally binned, Reproducible, and Pool-Adjacent-Violators algorithm based (CORP) decomposition of the BS (Dimitriadis et al. 2021; Loveday et al. 2024). CORP uses nonparameteric isotonic regression to robustly decompose BS into miscalibration MCB, discimination DSC and uncertainty $\mathrm{BS}^{\mathrm{ref}}$ terms,

$$\mathrm{BS} = \mathrm{MCB} - \mathrm{DSC} + \mathrm{BS}^{ref}. \tag{8}$$

Small values of MCB indicate that the forecast is reliable, in that the observed frequency of threshold exceedances for a given forecast probability matches that forecast probability. Larger values of DSC indicate that the forecast is able to better discriminate between exceedance and non-exceedance.

2.4.4 Cross validation and out of sample testing

We use a cross-validation approach to evaluate the skill of SOHTF at each tide gauge location across the hindcast period. This involves training the forecast system (i.e. computing tide predictions, residual climatologies, auto-correlation functions, ACCESS-S2 climatologies, sea level trends and percentile-based thresholds) on all but one year of data and verifying the forecast systems performance on that held-out year. This process is performed for every year of the hindcast at each location (a single "fold" of the cross-validation), with the results then averaged across all folds. While other choices of fold configurations are possible (e.g. holding out a random non-contiguous set of data), the choice of using a contiguous years yields a reasonable number of folds and is appropriate to the forecast use case where predictions are created for the upcoming year (using observed statistics from previous years).

2.4.5 Statistical significance

The Diebold-Mariano test (Diebold and Mariano 1995), with the Hering and Genton (2011) modification, on the time series of raw score differences (CRPS or BS) at each time and location is used to evaluate statistical significance of score differences. Following convention we use a $p = 0.05$ level for statistical significance.

3 Results: Skill assessment of SOHTF-CLIM

In this section we assess the skill of SOHTF-CLIM, the system without including ACCESS-S2 seasonal forecasts included [$i = 0$ in Eq. (1)]. We assess the skill of SOHTF-CLIM in predicting total water level (Sect. 3.1) as well as threshold exceedance probabilities (Sect. 3.2) at the Australian and western Pacific island sites (see Fig. 1a for site locations).

3.1 Total water level prediction skill

Total water level prediction skill for SOHTF-CLIM is assessed using the CRPS metric (shown averaged over all calendar months in Fig. 3a) and compared to two reference forecasts:

- a "climatological" probabilistic reference forecast, corresponding to the climatological distribution of total sea level observed at that location for the given month and,
- a "tide-only" deterministic reference forecast, which includes only the tide and trend components of SOHTF-CLIM [i.e. the first two lines of Eq. (1)].

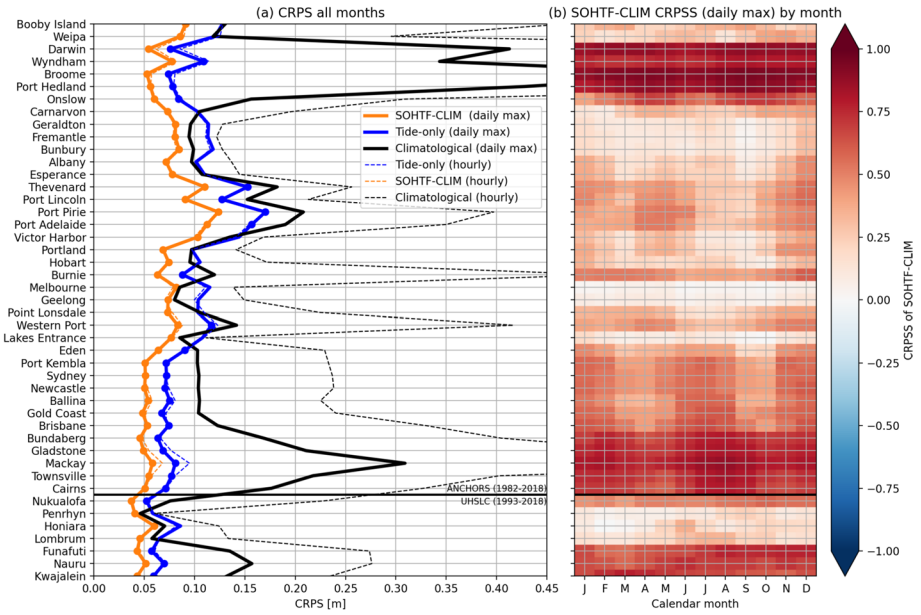

Fig. 3 CRPS verification of SOHTF-CLIM's total sea level forecasts. **a** CRPS for daily maximum (solid lines) and hourly (dashed lines) sea level forecasts averaged across all calendar months (smaller values are better). The black lines are for the climatological (distributional) reference forecast, the blue lines are for the tide-only (deterministic) reference forecast and the orange lines are for the SOHTF-CLIM (distributional) system. Dots indicate scores that are significantly better than the climatological forecast according to the Diebold-Mariano test ($p = 0.05$). **c** SOHTF-CLIM CRPSS of daily maximum sea level compared to the climatological reference as a function of calendar month (larger values are better). Verification is based on cross-validation across the 1982–2018 (ANCHORS) or 1993–2018 (UHSLC) periods (see methods)

As quantified using CRPS, the climatological reference forecast performs best where the overall sea level variability is smallest (black lines in Fig. 3a). Since this overall sea level variability is dominated by the tides at most locations, the climatological forecast performs worst in areas where the tidal range is large (Fig. 1a). For example, at Broome the CRPS for the climatological reference forecast reaches ~ 1.2m for hourly values and 0.6m for daily maximum values, while in Fremantle (relatively smaller tidal range) the CRPS for daily maximum sea level is only about 10 cm and at Penrhyn in the Pacific Islands it reaches as small as 5 cm.

The CRPS of the tide-only reference forecast (blue lines in Fig. 3a) is equal to the mean absolute error and thus to the time mean of the absolute value of the non-tidal residual. This is largest along the south coast of Australia where mid-latitude storm surges dominate (compare blue lines in Fig. 3a to Fig. 1c). For hourly sea level, the tide-only forecast performs better than the climatological forecast at all locations (compare dashed blue and black lines in Fig. 2a). However, in locations where tidal variability is smallest, the tide-only forecast performs worse than the climatological forecast for daily maximum sea level (e.g. Fremantle, Melbourne, Lakes Entrance and Penrhyn in the Pacific Islands, compare blue and black solid lines in Fig. 3a). This is because in these locations the non-tidal residual variability is a large fraction of the total sea level variability, and is not taken into account by the tide-only forecast. We also note that the CRPS for the tide-only forecast is very similar for both hourly and daily maximum sea level (compare dashed and solid blue lines in Fig. 3a), which suggests that non-linear interactions between the tide and the residual are of second order. These differences are largest at locations with complex tidal dynamics, such as Mackay on the Australian east coast.

SOHTF-CLIM, which includes climatological distributions of the non-tidal residual (rather than the climatological distribution of the total sea level for the climatological reference forecast), in addition to the tide-only forecast, performs better than both the tide-only forecast and the climatological reference forecasts at all locations for both hourly and daily maximum forecasts (compare orange, blue and black lines in Fig. 3a). The improvement over the tide-only forecast is consistently 3cm or larger, reaching 5cm along the south coast of Australia where non-tidal residual variability is largest. As a fraction of the tide-only forecast error, this improvement is close to 30% at all locations (i.e. the CRPSS of SOHTF-CLIM relative to the tide-only forecast remains within ± 0.02 of 0.29). Evaluated using the Diebold-Mariano test, SOHTF-CLIM's CRPS is significantly better than climatology at all locations (indicated by the orange dots in Fig. 3a), with the greatest improvements being where tide variability is largest. At most locations there is little seasonality in SOHTF-CLIM's CRPSS relative to the climatology for daily maximum sea level (Fig. 3b). Where seasonality is evident, it is partially related to variations in the magnitude of unpredictable residual variability (Fig. 2b), such as the reductions in skill in late winter along the southern Australian coast associated with winter storms and in austral late summer and winter in some of the Pacific islands.

3.2 Threshold exceedance skill

SOHTF-CLIM's skill for forecasts of the probability of exceeding the 99th percentile of daily maximum sea level is assessed using the BS, in comparison to two reference forecasts, the best constant reference forecast and a climatological reference forecast

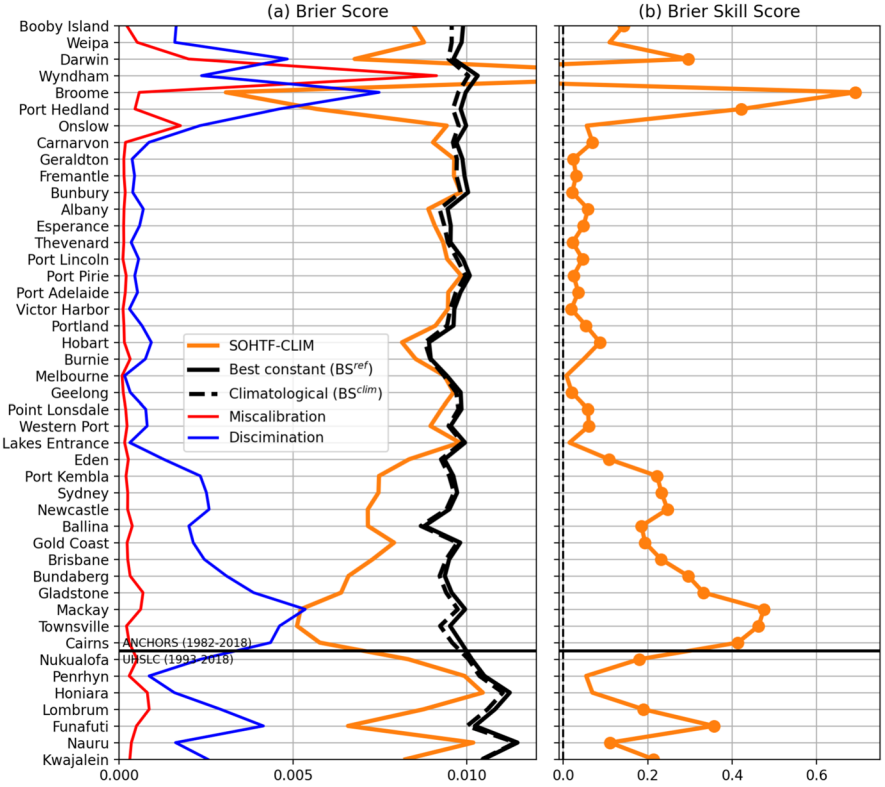

Fig. 4 Brier score verification for SOHTF-CLIM's forecasts of the probability of the daily maximum sea level exceeding the 99th percentile. **a** The BS for SOHTF-CLIM (orange), the best constant reference forecast (black solid line, BS^{ref}) and a climatological reference forecast (black dashed line). Also shown are the decomposition of SOHTF-CLIM's BS into CORP miscalibration (red) and discrimination (blue) terms. **b** The BSS of SOHTF-CLIM relative to the best constant reference forecast. Orange markers indicate that the BSS is statistically significant according to the Diebold-Mariano test ($p = 0.05$). Verification is based on cross-validation across the 1982–2018 (ANCHORS) and 1993–2018 (UHSLC) period (see methods)

computed based on the climatological frequency of observed threshold exceedances (e.g. Fig. 2d). Given the choice of a 99th percentile threshold, the best constant reference forecast probability is about 0.01. It only differs weakly from this value due to missing data and the fact that the 99th percentile thresholds are computed on a subset of the hindcast data and assessed on the remaining data using cross-validation (see methods Sect. 2.4.4). The corresponding BS^{ref} is also around 0.01 ($BS = (1 - p)p$ for $p = \overline{p^o}$ in Eq. (7), see black solid line in Fig. 4a)[1] Accounting for the seasonality in the observed threshold exceedance results in a slight improvement (compare black dashed

[1] Note that the reason that BS^{ref} is greater than 0.01 for the western Pacific islands, black lines in Fig. 4a, is because of the smaller record length and the dominance of interannual variability at these locations. This leads to single years in the record with high sea levels that correlate with low thresholds (because that year is excluded in the cross-validation process when computing the threshold), resulting in a higher average exceedance frequency (and thus BS^{ref}) over the cross-validation folds than expected from the 99th percentile threshold.

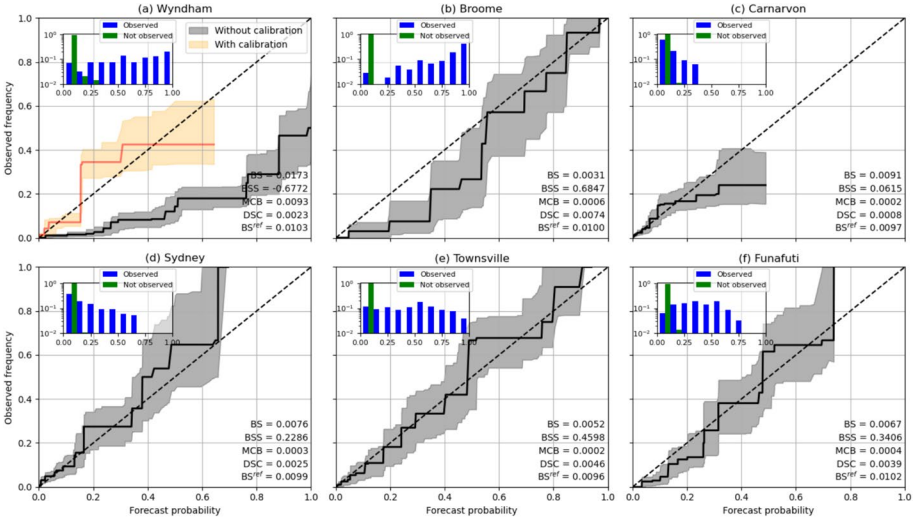

Fig. 5 Example CORP reliability diagrams for SOHTF-CLIM's forecasts of the probability of exceeding the 99th percentile of daily maximum total at a selection of tide gauge locations. The solid black lines show SOHTF-CLIM's CORP reliability curve (the observed frequency of threshold exceedance plotted against the forecast probability for threshold exceedance) computed via isotonic regression, with flat regions indicating where the forecasts have no discrimination. The dashed black lines indicate the line of perfect reliability. Gray shading indicates the 95% confidence interval around the reliability curve estimated using 250 bootstrapped samples. The inset plot shows a discrimination diagram with normalized histograms of the forecast probability when the threshold is exceeded (blue) or not (green) in the observations. The CORP summary BS, BSS, Miscalibration (MSC), Discrimination (DSC) and constant reference forecast BS (BS^{ref}) are shown within each panel. For Wyndham, the reliability diagram for the calibrated SOHTF-CLIM forecast (see Sect. 5), is also shown in red and orange

and solid lines in Fig. 4a). SOHTF-CLIM's BS is best at locations where tidal variability is largest (excluding Wyndham), along the north west, north east and east coasts and at some of the Pacific islands, and worst along the south Australian coast where the relative contribution of tides to the total variability is lowest (orange line in Fig. 4a). SOHTF-CLIM's BS is better than the best constant reference forecast at the majority of locations, as illustrated with the BSS (Fig. 4b). According to the Diebold-Mariano test, these differences are significant at all locations except for Wyndham, Onslow, Burnie, Melbourne, Lakes Entrance, Penrhyn and Honiara. Therefore, SOHTF-CLIM is expected to provide useful information about the probability of high water levels at most locations assessed in this study.

Performing a CORP decomposition of the BS allows us to better understand where SOHTF-CLIM's skill variations are coming from. The miscalibration term is small at most locations, indicating that the forecast probabilities are well calibrated (red line in Fig. 4a) in that the forecast probability matches the observed frequency of threshold exceedance well. This is better illustrated in reliability diagrams (Fig. 5) with SOHTF-CLIM's CORP reliability curve being close to the dashed one-to-one line of perfect reliability. At these locations where the forecast is well calibrated, variations in the BS are associated with the ability of the forecast to discriminate between threshold exceedances and non-exceedances (blue line in Fig. 4a). However, there are a few locations where SOHTF-CLIM's forecast probabilities are not well calibrated, the worst case

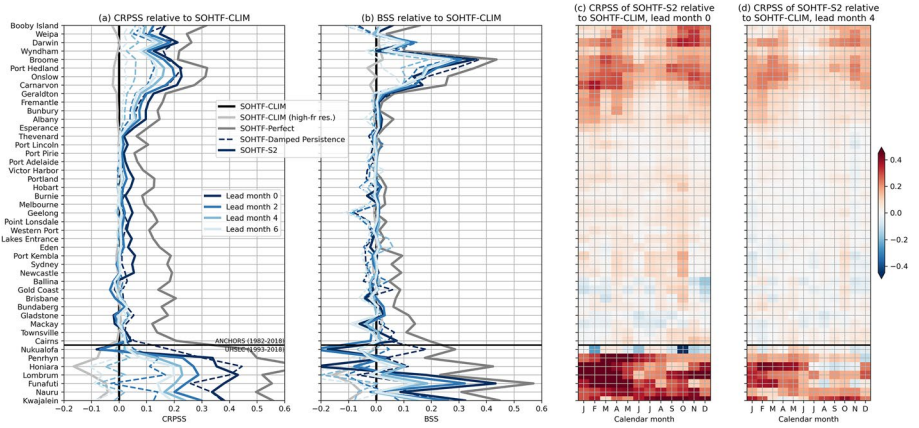

Fig. 6 **a** CRPSS of daily maximum sea level predictions and **b** BSS for threshold exceedance probability of 99th-percentile daily maximum relative to SOHTF-CLIM averaged over all calendar months for SOHTF-S2 predictions at lead months 0, 2, 4 and 6. CRPSS of SOHTF-S2 daily maximum sea level predictions as a function of calendar month at lead **c** 0 and **d** 4 months. Also shown in panels a and b are the scores for a version of SOHTF-CLIM that includes only high-frequency submonthly residuals in the residual distributions, a version with a perfect seasonal prediction (SOHTF-Perfect) where the monthly-mean residual is known exactly and for SOHTF-Damped Persistence forecasts at lead months 0, 2, 4 and 6

being Wyndham (black line in Fig. 5a). At Wyndham, SOHTF-CLIM tends to significantly over-predict the probability of threshold exceedance. However, the fact that discrimination is still positive at Wyndham (blue line in Fig. 4a), combined with the good CRPS skill for daily maximum sea level prediction (e.g. Fig. 3) suggests that a simple calibration of the forecast probabilities could improve skill at Wyndham. This possibility is explored in Sect. 5.

4 Results: impact of including ACCESS-S2 (SOHTF-S2)

We now assess whether including the ACCESS-S2 seasonal sea level anomaly forecasts, as a replacement for the monthly-mean residuals captured within the residual distributions in SOHTF-CLIM, improves the skill. This is done by computing the CRPSS and BSS of SOHTF-S2 relative to SOHTF-CLIM (Fig. 6), which quantify the fractional reduction in forecast error in SOHTF-S2 relative to SOHTF-CLIM. We assess these improvements at lead months 0, 2, 4 and 6, corresponding to the first, third, fifth and seventh months following the ACCESS-S2 forecast initialization date. The skill metrics are computed for daily maximum sea level forecasts averaged within the given lead month and across all calendar months (for Fig. 6a, b) or as a function of calendar month (for Fig. 6c, d).

Including ACCESS-S2 improves the CRPS of the daily maximum sea level forecast in regions where ACCESS-S2 has significant skill in forecasting monthly-mean sea level anomalies (see Holmes et al. (2025) for a detailed assessment). Within the first lead month, these improvements range between 10% and 23% along the north, north west and west coasts of Australia (dark blue line in Fig. 6a). In the tropical Pacific, improvements are even larger, reaching 43% at Lombrum. In this first lead month, the skill arises largely from the persistence of the monthly-mean sea level anomalies, with a simple damped persistence forecast (as used in Dusek et al. (2022), SOHTF-Damped Persistence, dashed lines

in Fig. 6) performing similarly to ACCESS-S2 at most locations. In the locations where persistence performs well in the first lead month, the improvements in SOHTF-S2 are a large fraction of the (unachievable) skill arising from a forecast where the monthly-mean anomalies were known exactly (dark gray line in Fig. 6a). However, along the south and east coasts of Australia the benefit of including the seasonal anomaly forecast (even if perfect) is much smaller as the seasonally-predictable, low-frequency sea level anomalies (see Figs. 1d, e, f) are only a small fraction of the total sea level variability (see Holmes et al. (2025) for a more detailed discussion, in particular their Fig. 1).

The improvements in the CRPS for SOHTF-S2 over SOHTF-CLIM are largely maintained out to lead month 6, particularly along the north west coast and in the Pacific islands (compare solid blue lines of different shading in Fig. 6a). This contrasts with SOHTF-Damped Persistence, whose skill decays much more rapidly with lead time (compare dashed and solid lines of different shading in Fig. 6a). Note there is evidence that SOHTF-S2's skill improvements might continue beyond the longest lead time shown in Fig. 6a, if ACCESS-S2 forecasts were available at longer lead times. However, we also note that when not using ACCESS-S2, including the monthly-mean residuals within the residual distribution rather than using submonthly residuals only does lead to a small improvement in CRPSS particularly in the western Pacific islands (light gray lines in Fig. 6a, b). Therefore, when implemented in real-time, predictions made beyond the last lead time available from ACCESS-S2 should revert to using the full residual distributions as in SOHTF-CLIM.

Moving on to the threshold exceedance forecasts, the improvements in the BSS of SOHTF-S2 over SOHTF-CLIM generally have a similar spatial pattern as for the CRPS, but are less pronounced as expected from the focus just on the highest sea levels (Fig. 6b). However, skill improvements exceeding 20% along the north west coast (up to 35% at Broome) and up to 40% in the tropical Pacific (Funafuti) are still observed, which in some cases is a larger improvement than for the CRPS. Throughout all of the south and east coasts SOHTF-S2 does not result in any improvement in BSS even in the first lead month, despite the improvement in CRPS (compare darkest blue line in Fig. 6a, b).

Finally, we note that the value of including ACCESS-S2 forecasts has a seasonal dependence when quantified using CRPS (Fig. 6c,d). At lead month 4 the benefit reduces for the months of May-August in Australia, consistent with the spring predictability barrier for ENSO prediction (Holmes et al. 2025).

5 Results: reliability calibration for threshold exceedance probability forecasts

As discussed in Sect. 3, SOHTF is well calibrated at most locations but there are some exceptions. The worst case is Wyndham, where the forecast probabilities are significantly over-predicted (black lines in Fig. 5a). At Wyndham, the tide prediction over-predicts many of the highest high tides. This is illustrated in Fig. 7, where there is a distinct negative anomaly in the non-tidal residual at the times of the peak daily high tide over an example 4 day period. This over prediction arises because the Wyndham tide gauge is located within a complex estuary with narrow passages, shallow topography and strong riverine flows. Harmonic tide predictions at this location struggle to capture the associated non-linear residual-tide interactions (Speer and Aubrey 1985; Parker 2007). It is of note that this over-prediction is not corrected by the simple tidal decile dependence included in the residual statistics computation (e.g. Fig. 2c). This is because the highest high tides that result in

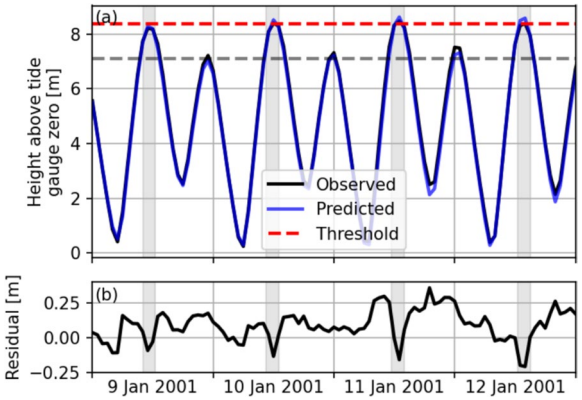

Fig. 7 Hourly observed sea level (black in panel a), SOHTF-CLIM predicted mean sea level (blue in panel a), 99th percentile of daily maximum threshold (red dashed in a) and observed non-tidal residual (panel b) at the Wyndham tide gauge for four days between the 9th of January 2001 and the 12th of January 2001. Gray shading highlights the daily high high tide times, where there is a distinct negative anomaly in the non-tidal residual. The gray dashed line in panel a denotes the lower bound of the top tidal decile at Wyndham

threshold exceedence occur only within the top fraction of the top tidal decile (denoted by the gray dashed line in Fig. 7).

To address this issue, we used isotonic regression to calibrate the forecast probabilities. The calibration uses the reliability curve (e.g. Fig. 5a) computed within the given training period (i.e. all but one year of the hindcast in the cross-validation process) as a rescaling to adjust the forecast probabilities such that the observed frequency of threshold exceedances matches the forecast probabilities within this training period. The scaling is then applied to the probability predictions in the prediction period (the left out year in the cross-validation process).

When computed and tested using cross-validation, the calibration strongly improves the reliability of the forecast probabilities at Wyndham, as expected (compare black and orange reliability curves in Fig. 5). The miscalibration is largely removed and the BSS becomes positive and significant (compare orange and green lines in Figs. 8a,b). While the biggest improvement is at Wyndham, the calibration also improves the BSS at Darwin, Onslow, Burnie, Gladstone, Mackay, Nukualofa and Honiara. Like Wyndham, some of these locations are also characterized by shallow, complex topography and tidal dynamics. In most locations both within and outside this set, there is little change in discrimination (Fig. 8c). This may be because isotonic regression ensures that the calibration scaling does not negatively impact discrimination if tested within the training period (as opposed to a more ad-hoc binning method). However, in some locations, such as Sydney and Honiara for example, the improvement in calibration is partially or completely compensated by a decrease in discrimination, resulting in little change in the BSS. Note that this calibration step can only be applied to improve the threshold exceedance forecasts, not the total sea level forecasts.

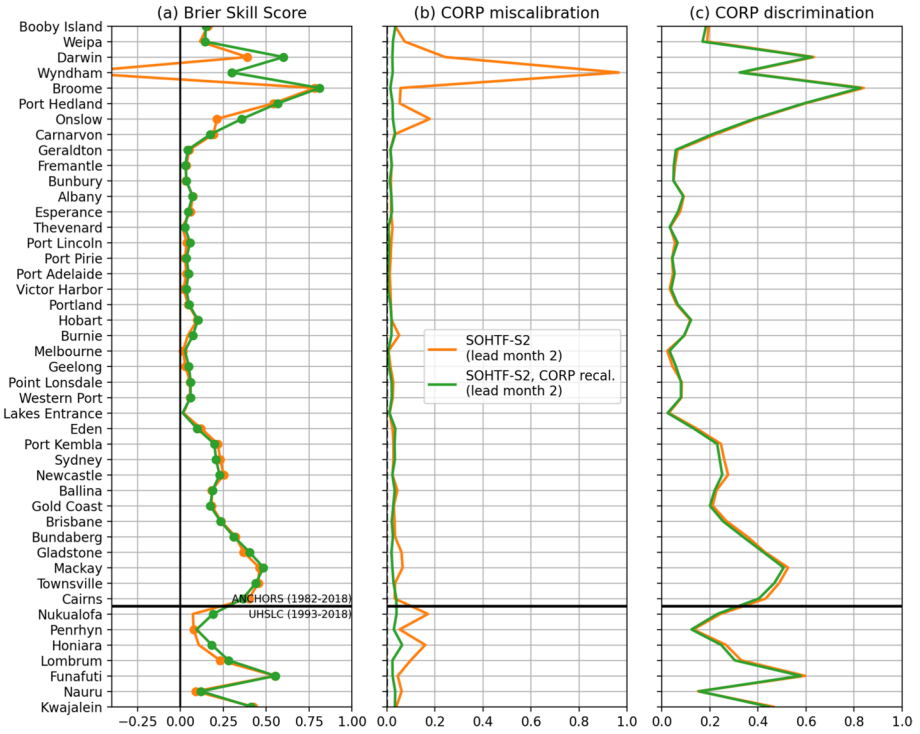

Fig. 8 **a** BSS (relative to the best constant reference forecast) and CORP, **b** miscalibration and **c** discrimination terms for SOHTF-S2 forecasts (at lead month 2) of the probability of exceeding the 99th percentile of daily maximum sea level at each tide gauge location computed using cross-validation across the hindcast period. The orange lines do not include reliability calibration while the green lines do. Dots in panel a indicate that the BSS (relative to the best constant reference forecast) is statistically significant according to the Diebold-Mariano test ($p = 0.05$)

6 Skill dependence on threshold

The skill assessments provided above have used the 99th percentile of the daily maximum total sea level for the threshold exceedance forecasts. However, the choice of relevant threshold is highly application and user dependent. Our intention is to provide a flexible system that can be used with a range of thresholds chosen based on the specific needs of the user. In this section we explore the sensitivity of the forecast skill to the threshold in both SOHTF-CLIM and SOHTF-S2.

As expected, the BSS of SOHTF-CLIM relative to the best constant reference forecast decays for rarer, more extreme events, as these events are driven by extreme storm surges associated with chaotic, weather-driven variability that is not predictable at seasonal time scales (Fig. 9b, consistent with Dusek et al. 2022). While skill is significant at all stations for the 95th percentile thresholds and at most stations for the 99th percentile (as assessed earlier), skill is only significant for parts of the north west coast and most of the east coast at the 99.5th percentile (corresponding to flooding that occurs 1.8 days a year on average). At the 99.9th percentile, corresponding to an event occurring on average once every three years, SOHTF-CLIM has no skill at any location.

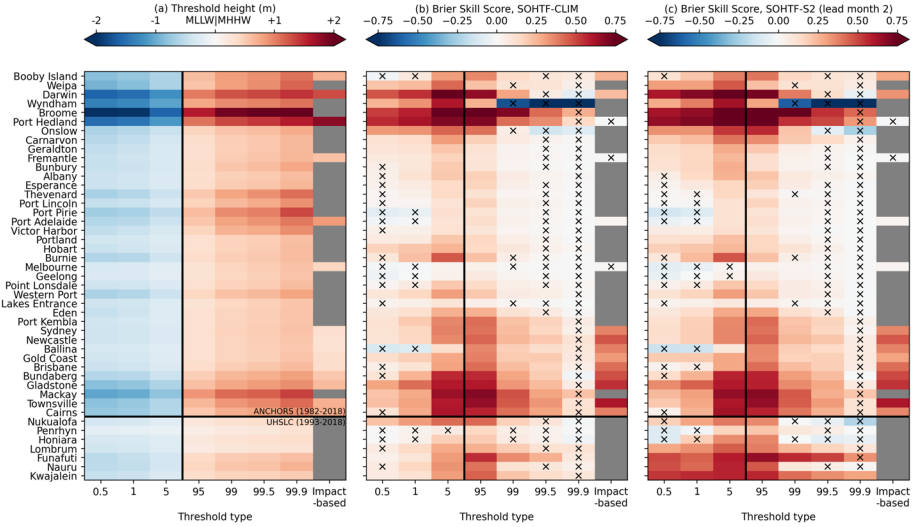

Fig. 9 **a** Threshold height and BSS relative to the best constant reference forecast for (**b**) SOHTF-CLIM and (**c**) SOHTF-S2 at lead month 2. The threshold heights in panel a are plotted relative to Mean Higher High Water (MHHW, the mean of the daily maximum tide over the hindcast period) for percentiles above 50 and relative to Mean Lower Low Water (MLLW, the mean of the daily minimum tide over the hindcast period) for percentiles below 50. We consider frequency-based thresholds based on 0.5, 1 and 5-th percentiles for daily minimum sea level, and the 95, 99 (as used earlier in the article), 99.5 and 99.9-th percentiles for daily maximum sea level. The last column shows the BSS for exceedance forecasts of the impact-based minor flooding thresholds from Hague et al. (2022) where they are available. Black crosses indicate scores that are not statistically better than the best constant reference forecast according to the Diebold-Mariano test ($p = 0.05$). Note that these forecasts are not calibrated

SOHTF-CLIM's skill for impact-based minor flooding thresholds, available for a subset of Australian locations from Hague et al. (2022), depends on the relative frequency at which they are exceeded (compare impact-based with frequency-based threshold heights in Fig. 9a). Encouragingly, SOHTF has skill for most of the locations with well-defined impact-based minor flooding thresholds, which are mainly along the east coast where these thresholds are exceeded relatively frequently. Note that we have not included locations with "poor-quality" impact-based minor flooding thresholds (listed with superscript 'a' in Table 2 of Hague et al. (2022)), which were defined based on less than 10 flooding event reports.

We have also assessed the skill of SOHTF in predicting occurrence probabilities for low-water events (left of solid vertical line in Fig. 9). Overall, the skill for low-water events is similar to high-water events for an equivalent event frequency. However, there are some locations where the skill differs significantly. For example, at Ballina and at a few of the Pacific islands (e.g. Funafuti), low-water events are much less predictable using SOHTF-CLIM than high-water extremes. In the Pacific islands, skill for low-water events is largely recovered in SOHTF-S2 (Fig. 9c) further highlighting the important role of seasonal variability at these locations (but not at Ballina, where the seasonally predictable low-frequency signal is negligible, see Figs. 1e, f and Holmes et al. 2025). At some locations, such as Hobart, Burnie and Wyndham, the skill for low-water events is higher than for high-water events. These differences may be associated with non-linearities in the tidal dynamics. For example, the complex tidal

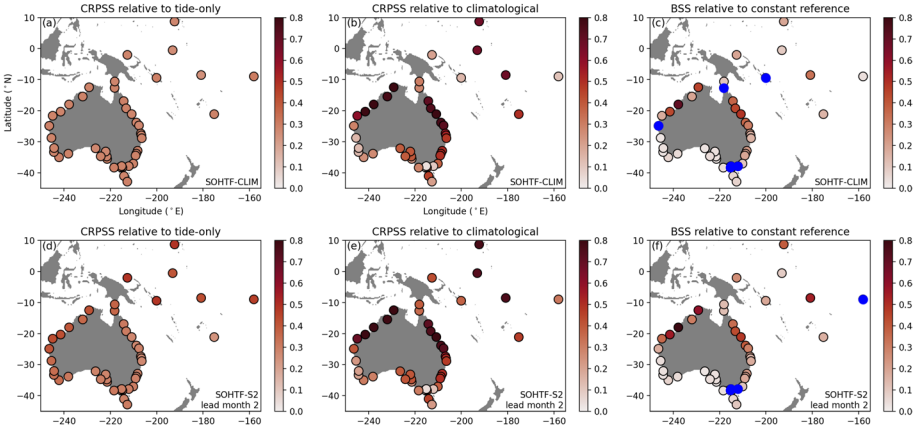

Fig. 10 CRPSS relative to (**a**, **d**) tide-only and (**b**, **e**) climatological forecasts and (c,f) BSS relative to the best constant reference forecast. Panels a–c are for SOHTF-CLIM, while panels d-f are for SOHTF-S2 at lead month 2, and all include the reliability calibration from Section 5. Blue dots (in all panels) indicate locations where the skill is not significant (at the $p = 0.05$ level according to the Diebold-Mariano test) compared to the given reference forecast

dynamics at Wyndham responsible for the lack of skill for high-water events (without the calibration discussed in Sect. 5) does not affect the predictability of low-water events, which are well predicted. More work is needed to better understand the dynamics driving low-water extremes and how they differ from high-water extremes.

7 Summary and discussion

In this study we have developed and assessed the performance of a probabilistic seasonal forecast system for coastal sea level at tide gauges around the Australian coast and in the western Pacific islands, the Seasonal Outlooks for High Tide Flooding (SOHTF) system. SOHTF is a blended system that combines deterministic tide predictions, sea level rise projections, probabilistic representations of residual variability and dynamical seasonal sea level anomaly ensemble forecasts from ACCESS-S2 (see Section 2). It provides probabilistic forecasts of total sea level and threshold exceedance probability at daily time scales from 1 to 8 months lead time (SOHTF-S2) and beyond (SOHTF-CLIM).

We first showed that including climatological distributions of the non-tidal residual variability on top of a tide-only forecast can reduce the forecast error for daily maximum sea level, as measured by the CRPS, by about 30% at all locations (Figs. 3, 10a). This constitutes a simple method for improving tide predictions, and yields improvements that are comparable or better than what can be achieved by optimising the tide prediction itself (e.g. Richet et al. 2024). SOHTF-CLIM produces a probabilistic forecast for daily maximum sea level that performs best for locations with large tidal ranges and weak residual variability (Figs. 3a, 1, 10b). These results suggests that probabilistic tide forecasts that account for the climatological magnitude of non-tidal residual variability should be explored further as a tool for improving tide predictions in general.

We then demonstrated that SOHTF is skilful in predicting the probability of exceeding the 99th percentile of daily maximum total water level, representative of high-tide

flooding frequencies, at most locations (Figs. 4, 10c). We showed that including seasonal anomaly forecasts from ACCESS-S2 (SOHTF-S2) led to improvements of between 10% and 23% in CRPS and up to 35% BS for daily maximum sea level (but generally much less) on the north and west coasts of Australia (Sect. 4, Fig. 6, also compare the first and second rows of Fig. 10). However, this approach resulted in negligible improvements on the south and east coasts, and any skill improvements decreased with lead time. Even larger improvements were seen in the western Pacific islands. We also showed that including a simple calibration step, based on the reliability curve of hindcast probabilities, can improve the forecast skill at locations with complex, non-linear tidal dynamics such as Wyndham (Section 5, Fig. 8). When all improvements are applied, the CRPSS of SOHTF relative to a climatological forecast generally ranges between values of 0.2 along the south coast of Australia (reaching as low as 0.04 in Melbourne due to the small tidal variability and dominance of unpredicatable weather-driven dynamics) to 0.8 and above in the north-west, north-east and western Pacific islands out to a lead time of 3 months (Fig. 10e). The BSS for 99th percentile daily maximum threshold exceedance at this lead time is significant at all 46 locations except for Melbourne, Lakes Entrance and Penrhyn. It reaches values above 0.25 at many sites on the north west and north east coasts (Fig. 10f). Finally, we also showed that SOHTF's skill is sensitive to the choice of threshold with skill decaying for higher thresholds that are exceeded less frequently (Fig. 9). Encouragingly, SOHTF has skill for impact-based minor flooding threshold exceedance at most of the locations where these thresholds are defined.

The implementation of SOHTF in a real-time setting is currently under development and will require several additional considerations beyond those presented here. These include the treatment of sea level trends (see Appendix A) including the role of vertical land motion (ignored here), the use of ACCESS-S2's real-time forecast system (which includes 99 ensemble members and more start dates than the hindcast system assessed here; see Wedd et al. (2022)) and the updating of statistical distributions and tidal epochs when new data becomes available. These considerations will be described in a future publication.

SOHTF has a number of potential applications for user groups ranging from local councils, meteorological agencies and emergency services to coastal ecosystem managers and the general public. To meet the needs of this diverse group of potential users, a number of forecast products are under development. These range from simplified tide-table type calendar visualizations for the upcoming year (as discussed by Dusek et al. (2022)), maps highlighting which locations are at most risk of flooding for any particular future day (not shown), to dynamic site-based time series products (e.g. Fig. 11). Other products beyond the daily time-scale could also be considered, such as seasonal outlooks that aggregate risk of threshold exceedance by month or season.

SOHTF is flexible in terms of the threshold chosen and can be tailored to ensure that the forecasts are both skillful and relevant to the user (Fig. 9). However, the development of meaningful, impact-based or user-focused thresholds is in itself an important, under-appreciated topic (e.g. Sweet 2018; Hague et al. 2022; Rasmussen et al. 2022; Mahmoudi et al. 2024). Furthermore, as noted by Dusek et al. (2022), as sea levels rise in the future the predictability of high-water events for a fixed threshold are expected to improve. Flooding will increasingly arise solely due to predictable factors such as the tides and seasonal anomalies (Hague et al. 2023; Hague and Talke 2024). Sea level rise has already occurred, suggesting that our skill estimates for 99th percentile thresholds averaged over the entire hindcast period correspond to a lower bound on the current real-time skill of SOHTF for those same thresholds. SOHTF is skillful

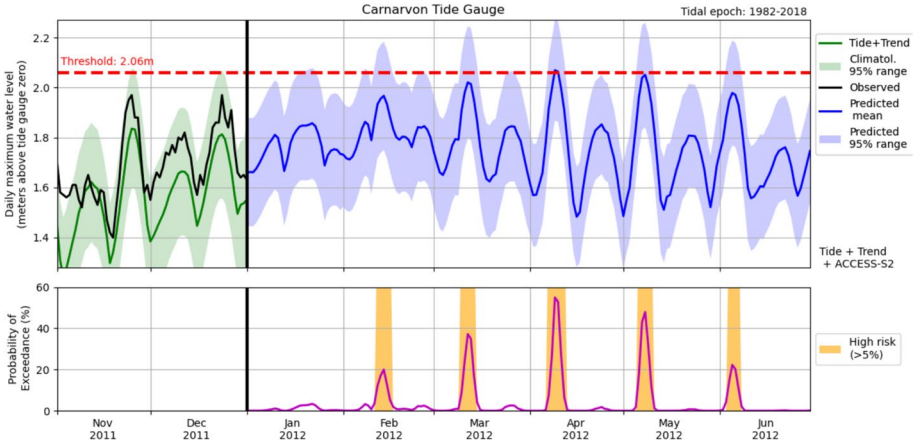

Fig. 11 An example time series product for a SOHTF forecast (trained on statistics over the full 1982–2018 hindcast period) for daily maximum sea level (top panel) and probability of exceeding the threshold of 2.06m above tide gauge zero (bottom panel) for the Carnarvon tide gauge in Western Australia made at the end of 2011 for the first six months of 2012. The top panel shows observations (black), the tide (+ trend) prediction and climatological 95% residual range (green) in the past, as well as the forecast mean and 95% range for the future (blue line and shading). This forecast includes ACCESS-S2 which, due to the ongoing and forecast 2011–2012 La Nina event, predicts higher than normal sea level anomalies accounting for the jump between the tide prediction (green) and the forecast mean (blue) at the end of December 2011. The bottom panel shows the forecast probability of exceeding the threshold (red dashed line in the top panel, which can be chosen dynamically be the user) with high risk periods above 5% highlighted in yellow

for events that occur a couple of times per year on average, a frequency often used as an adaptation trigger under an "accommodate" adaptation pathway (e.g. Barnett et al. 2014; Buchanan et al. 2019; Ayşın Dedekorkut-Howes et al. 2021). If such a pathway is chosen, SOHTF could help identify whether, when and where temporary measures to accommodate flood hazards may be needed in a forthcoming season. With this aim, the products developed from SOHTF will be used in conjunction with gridded seasonal forecast information from ACCESS-S2 alone (Holmes et al. 2025) to form an operational service to inform decision making and improve community resilience to coastal flooding hazards.

There are a number of potential extensions to SOHTF that could be explored in future work. Firstly, the assumption of normality in the residual distributions could be relaxed, with the possibility of using either the empirical historical distribution or skew-normal or other parameteric distributions that may better characterize the extremes to improve forecast skill. Secondly, most users are interested in the forecast for their location, rather than at a tide gauge that may be far away. The relevance of a forecast at a tide gauge for nearby flooding impacts depends on the local topography, and again highlights the need for the development of relevant thresholds that translate the water level observed at a tide gauge to the impacts felt in nearby locations. A gridded version SOHTF, based on gridded tide predictions and residual distributions computed from high-resolution coastal hindcast simulations (e.g. Rose et al. 2024; Operational Oceanographic Products et al. 2025), could provide more useful predictions to a greater range of stakeholders, if found to be skillful. Thirdly, the development of seamless forecasts which blend SOHTF with subseasonal forecasts (available from ACCESS-S2 for lead weeks 0-5) and/or days 0-6 storm surge forecasts (e.g. Taylor and

Brassington 2017) using statistical techniques would provide users with information across time-scales to enable continuous decision making (also see Neal et al. 2018). Finally, SOHTF could be applied in a future projections context to understand interactions between seasonal, tidal, residual and relative sea level rise components of sea level variability and their impacts on future flood risk.

Appendix A: Additional improvements explored

Here we list additional factors that we considered in this study but which did not lead to any significant improvements in SOHTF's forecast skill.

1. Using ACCESS-S2's prediction for the submonthly variance of sea level (using available daily forecast data) as an alternative to using climatological non-tidal residual distributions. However, a preliminary skill analysis revealed that ACCESS-S2 has little skill in predicting variations in the submonthly (daily) variance of sea level beyond the climatology.
2. Not including the annual and semi-annual constituents *Sa* and *Ssa* in the tide prediction, and thus capturing the seasonal cycle implicitly in the non-tidal residual distribution means. This would correspond to a climatological (rather than sinusoidal) seasonal cycle, and was advocated for by Stephens et al. (2014) based on arguing that *Sa* and *Ssa* are difficult to predict ahead of time. This was tested within the cross-validation hindcast set and found to have little impact on forecast skill except in the Gulf of Carpentaria (the Weipa and Booby Island gauges), where the seasonal cycle is particularly strong. At these locations the skill was slightly worse when relying on the climatological seasonal cycle, and thus *Sa* and *Ssa* were retained in the tidal prediction (see Richet et al. (2024) for a detailed study of the sensitivity to various tidal prediction configurations).
3. Using a variance inflation calibration step to correct for biases in ACCESS-S2's representation of the magnitude of monthly mean sea level variability. These biases include a slight underestimate of variability on the north and north west coasts, and an overestimate of variability along the south coast (see Holmes et al. (2025)). To correct for these biases, we scaled the magnitude of the ACCESS-S2 sea level anomalies so that their amplitude matched the observed variability. However, when assessed using the cross-validated hindcast set, the relative improvement in CRPS and BS under the calibration was weak ($< 7\%$ at most stations) and not consistently positive. Therefore, we choose not to use this calibration option.
4. Using a multi-linear regression approach to account for the impact of climate variability on local sea level rise rates. The deterministic relative sea level rise component used here is a simple quadratic (for the ANCHORS gauges) or linear (for the western Pacific island gauges) regression over the hindcast period. However, when computed over relatively short periods (i.e. particularly for the western Pacific island gauges with the shorter 1993–2018 hindcast period) these trends can be impacted by climate variability. For example, the transition from a positive to a negative phase of the Interdecadal Pacific Oscillation before and after the turn of the century is known to have masked the background accelerating sea level rise in many regions of the western Pacific and along the northern coast of Australia (Wang et al. 2021). In a real-time prediction system, projecting forward the trend computed over a period spanning this transition could lead to an underestimation of the rate of sea level rise in the future if the IPO reverses sign.

To address this issue, we considered computing the trend using a multi-linear regression that includes the Niño 3.4 index and the tripole index for the IPO (Henley et al. 2015) as additional predictors (following Wang et al. 2021), in order to remove their impact on the trend. When tested over the 2019–2022 period (appropriate for a real-time application) the results of this approach were mixed, with an apparent strong dependence on the fact that this period is La Niña dominated. Therefore, we choose not to present these results here, but this option could be explored further when applying this forecast system in a real-time operational setting.

5. Accounting for the observed past modulation of the high-frequency residual standard deviation by ENSO, along with ACCESS-S2's ENSO predictions, as an attempt to account for the impact of ENSO on storminess. This was evaluated by computing the residual standard deviation at each tide gauge separately for quintiles of the Niño 3.4 index, with the intention of then altering the residual standard deviation in the prediction system according to this relationship and ACCESS-S2's prediction of the Niño 3.4 index. However, we found that the relationship between the high-frequency residual standard deviation and the Niño 3.4 index was relatively weak (less than 10% at most locations) and inconsistent across locations. A similar calculation for the Southern Annular Mode illustrated some connection to sea level variability along the south Australian coast, but in this case seasonal predictability of SAM is quite weak (also see Holmes et al. (2025)). Therefore, we choose not to further pursue this option in this study.

Acknowledgements The authors acknowledge the use of the National Computational Infrastructure (NCI) which is supported by the Australian Government. We thank the Bureau of Meteorology seasonal prediction teams for their work developing and maintaining ACCESS-S2. We acknowledge the developers of the SCORES (Leeuwenburg et al. 2024, https://github.com/nci/scores) forecast verification package. We thank Rob Taggart for assistance with verification metrics and reviewers Nicholas Loveday and Andy Taylor (Bureau of Meteorology) for their early reviews and feedback.

Author Contributions R. Holmes conceived the study, performed the analyses and wrote the initial draft. All authors contributed to the drafting of the final manuscript.

Funding This research was funded by the Australian Climate Service.

Data availability ACCESS-S2 hindcast data is available at https://dx.doi.org/10.25914/60627ad0ba3ee. ANCHORS tide gauge data is available at https://dx.doi.org/10.25914/6142dff37250b. UHSLC tide gauge data is available at https://uhslc.soest.hawaii.edu/data/.

Declarations

Conflict of interest The authors have no relevant financial or non-financial interests to disclose.

References

Abhik S, Hope P, Hendon HH, Hutley LB, Johnson S, Drosdowsky W, Brown JR, Duke NC (2021) Influence of the 2015–2016 El Niño on the record-breaking mangrove dieback along northern Australia coast. Sci Rep 11(1):20411. https://doi.org/10.1038/s41598-021-99313-w

Allison AEF, Lawrence JH, Stephens SA, Kwakkel JH, Singh SK, Blackett P, Stroombergen A (2024) Planning for wastewater infrastructure adaptation under deep uncertainty. Front Clim. https://doi.org/10.3389/fclim.2024.1355446

Ampou EE, Johan O, Menkes CE, Niño F, Birol F, Ouillon S, Andréfouët S (2017) Coral mortality induced by the 2015–2016 El-Niño in Indonesia: the effect of rapid sea level fall. Biogeosciences 14(4):817–826. https://doi.org/10.5194/bg-14-817-2017

Ayşın Dedekorkut-Howes ET, Howes M (2021) Planning for a different kind of sea change: lessons from Australia for sea level rise and coastal flooding. Climate Policy 21(2), 152–170. https://doi.org/10.1080/14693062.2020.1819766

Barnett J, Graham S, Mortreux C, Fincher R, Waters E, Hurlimann A (2014) A local coastal adaptation pathway. Nat Clim Chang 4(12):1103–1108. https://doi.org/10.1038/nclimate2383

Brown BE, Dunne RP, Somerfield PJ, Edwards AJ, Simons WJF, Phongsuwan N, Putchim L, Anderson L, Naeije MC (2019) Long-term impacts of rising sea temperature and sea level on shallow water coral communities over a 40 year period. Sci Rep 9(1):8826. https://doi.org/10.1038/s41598-019-45188-x

Buchanan MK, Oppenheimer M, Parris A (2019) Values, bias, and stressors affect intentions to adapt to coastal flood risk: a case study from New York City. Weather Clim Soc 11(4):809–821. https://doi.org/10.1175/WCAS-D-18-0082.1

Caldwell PC, Merrifield MA, Thompson PR (2001) Sea level measured by tide gauges from global oceans as part of the Joint Archive for Sea Level (JASL) since 1846. Dataset. NOAA National Centers for Environmental Information. https://doi.org/10.7289/v5v40s7w. https://uhslc.soest.hawaii.edu/data/

Callaghan J, Power SB (2014) Major coastal flooding in southeastern Australia, associated deaths and weather systems. Aust Meteor Ocean J 64(3):183–213. https://doi.org/10.1071/ES14017

Codiga DL (2011) Unified tidal analysis and prediction using the UTide Matlab functions https://doi.org/10.13140/RG.2.1.3761.2008

Cooley S, Schoeman D, Bopp L, Boyd P, Donner S, Ghebrehiwet DY, Ito S-I, Kiessling W, Martinetto P, Ojea E, Racault M-F, Rost B, Skern-Mauritzen M (2022) In: Pörtner H-O, Roberts DC, Tignor M, Poloczanska ES, Mintenbeck K, Alegría A, Craig M, Langsdorf S, Löschke S, Möller V, Okem A, Rama B (eds), Oceans and coastal ecosystems and their services in climate change 2022 impacts, adaptation and vulnerability: working group II Contribution to the sixth assessment report of the intergovernmental panel on climate change, pp 379–550. Cambridge University Press, Cambridge. https://doi.org/10.1017/9781009325844.005

Department of Climate Change, Energy, the Environment and Water: National Climate Risk Assessment first pass assessment report. DCCEEW 2024 (2024). https://www.dcceew.gov.au/climate-change/publications/ncra-first-pass-risk-assessment. Canberra, March. CC BY 4.0

Diebold FX, Mariano RS (1995) Comparing predictive accuracy. J Bus Econ Stat 13(3):253–263. https://doi.org/10.1198/073500102753410444

Dimitriadis T, Gneiting T, Jordan AI (2021) Stable reliability diagrams for probabilistic classifiers. Proc Natl Acad Sci 118(8):2016191118. https://doi.org/10.1073/pnas.2016191118

Dusek G, Sweet WV, Widlansky MJ, Thompson PR, Marra JJ (2022) A novel statistical approach to predict seasonal high tide flooding. Front Mar Sci 9:1. https://doi.org/10.3389/fmars.2022.1073792

Enríquez AR, Wahl T, Baranes HE, Talke SA, Orton PM, Booth JF, Haigh ID (2022) Predictable changes in extreme sea levels and coastal flood risk due to long-term tidal cycles. J Geophys Res Oceans 127(4):e2021JC018157. https://doi.org/10.1029/2021JC018157

Flood JF, Cahoon LB (2011) Risks to coastal wastewater collection systems from sea-level rise and climate change. J Coastal Res 27(4):652–660. https://doi.org/10.2112/JCOASTRES-D-10-00129.1

Frankcombe LM, McGregor S, England MH (2015) Robustness of the modes of Indo-Pacific sea level variability. Clim Dyn 45(5):1281–1298. https://doi.org/10.1007/s00382-014-2377-0

Gneiting T, Katzfuss M (2014) Probabilistic forecasting. Ann Rev Stat Appl 1(1):125–151. https://doi.org/10.1146/annurev-statistics-062713-085831

Gneiting T, Raftery AE, Westveld AH, Goldman T (2005) Calibrated probabilistic forecasting using ensemble model output statistics and minimum crps estimation. Mon Weather Rev 133(5):1098–1118. https://doi.org/10.1175/MWR2904.1

Hague B, Talke S (2024) The Influence of Future Changes in Tidal Range, Storm Surge, and Mean Sea Level on the Emergence of Chronic Flooding. Earth's Future 12:. e2023EF003993. https://doi.org/10.1029/2023EF003993

Hague BS, McGregor S, Murphy BF, Reef R, Jones DA (2020) Sea Level Rise Driving Increasingly Predictable Coastal Inundation in Sydney. Australia Earth's Future 8(9):e2020EF001607. https://doi.org/10.1029/2020EF001607

Hague BS, Jones DA, Jakob D, McGregor S, Reef R (2022) Australian coastal flooding trends and forcing factors. Earth's Future 10(2):e2021EF002483. https://doi.org/10.1029/2021EF002483

Hague BS, Jones DA, Trewin B, Jakob D, Murphy BF, Martin DJ, Braganza K (2022) ANCHORS: a multi-decadal tide gauge dataset to monitor Australian relative sea level changes. Geosci Data J 9(2):256–272. https://doi.org/10.1002/gdj3.136

Hague BS, Grayson RB, Talke SA, Black MT, Jakob D (2023) The effect of tidal range and mean sea-level changes on coastal flood hazards at Lakes Entrance, south-east Australia. JSHESS. https://doi.org/10.1071/ES22036

Hague BS, Jakob D, Kirezci E, Jones DA, Cherny IL, Stephens SA (2024) Future frequencies of coastal floods in Australia: a seamless approach and dataset for visualising local impacts and informing adaptation. JSHESS. https://doi.org/10.1071/ES23024

Haigh ID, Eliot M, Pattiaratchi C (2011) Global influences of the 18.61 year nodal cycle and 8.85 year cycle of lunar perigee on high tidal levels. J Geophys Res Oceans. https://doi.org/10.1029/2010JC006645

Hamlington BD, Bellas-Manley A, Willis JK, Fournier S, Vinogradova N, Nerem RS, Piecuch CG, Thompson PR, Kopp R (2024) The rate of global sea level rise doubled during the past three decades. Commun Earth Environ 5(1):601. https://doi.org/10.1038/s43247-024-01761-5

Hanslow DJ, Morris BD, Foulsham E, Kinsela MA (2018) A regional scale approach to assessing current and potential future exposure to tidal inundation in different types of estuaries. Sci Rep 8(1):7065. https://doi.org/10.1038/s41598-018-25410-y

Hauer M, Mueller V, Sheriff G, Zhong Q (2021) More than a nuisance: Measuring how sea level rise delays commuters in miami, fl. Environ Res Lett 16(6):064041

Henley BJ, Gergis J, Karoly DJ, Power S, Kennedy J, Folland CK (2015) A tripole index for the interdecadal Pacific oscillation. Clim Dyn 45(11–12):3077–3090. https://doi.org/10.1007/s00382-015-2525-1

Hering AS, Genton MG (2011) Comparing spatial predictions. Technometrics 53(4):414–425. https://doi.org/10.1198/TECH.2011.10136

Hersbach H (2000) Decomposition of the continuous ranked probability score for ensemble prediction systems. Weather Forecast 15(5):559–570. https://doi.org/10.1175/1520-0434(2000)015<0559:DOTCRP>2.0.CO;2

Hino M, Belanger ST, Field CB, Davies AR, Mach KJ (2019) High-tide flooding disrupts local economic activity. Sci Adv 5(2):2736. https://doi.org/10.1126/sciadv.aau2736

Holmes RM, Smith GA, Spillman CM (2025) Seasonal sea level forecasts for the Australian coast. J South Hemisph Earth Syst Sci. https://doi.org/10.1071/ES24047

Hudson D, Alves O, Hendon HH, Lim E-P, Liu G, Luo J-J, MacLachlan C, Marshall AG, Shi L, Wang G et al (2017) ACCESS-S1 The new Bureau of Meteorology multi-week to seasonal prediction system. J South Hemisph Earth Syst Sci 67(3):132–159. https://doi.org/10.1071/ES17009

Kasmalkar IG, Serafin KA, Miao Y, Bick IA, Ortolano L, Ouyang D, Suckale J (2020) When floods hit the road: resilience to flood-related traffic disruption in the San Francisco Bay Area and beyond. Sci Adv 6(32):2423. https://doi.org/10.1126/sciadv.aba2423

Leeuwenburg T, Loveday N, Ebert EE, Cook H, Khanarmuei M, Taggart RJ, Ramanathan N, Carroll M, Chong S, Griffiths A, Sharples J (2024) scores: a python package for verifying and evaluating models and predictions with xarray. J Open Source Softw 9(99):6889. https://doi.org/10.21105/joss.06889

Long X, Widlansky MJ, Spillman CM, Kumar A, Balmaseda M, Thompson PR, Chikamoto Y, Smith GA, Huang B, Shin C-S, Merrifield MA, Sweet WV, Leuliette E, Annamalai HS, Marra JJ, Mitchum G (2021) Seasonal forecasting skill of sea-level anomalies in a multi-model prediction framework. J Geophys Res Oceans. https://doi.org/10.1029/2020JC017060

Loveday N, Taggart R, Khanarmuei M (2024) A user-focused approach to evaluating probabilistic and categorical forecasts. Weather Forecast 39(8):1163–1180. https://doi.org/10.1175/WAF-D-23-0201.1

Lowe RJ, Cuttler MVW, Hansen JE (2021) Climatic drivers of extreme sea level events along the coastline of Western Australia. Earth's Future 9(4):e2020EF001620. https://doi.org/10.1029/2020EF001620

Mahmoudi S, Moftakhari H, Muñoz DF, Sweet W, Moradkhani H (2024) Establishing flood thresholds for sea level rise impact communication. Nat Commun 15(1):4251. https://doi.org/10.1038/s41467-024-48545-1

McInnes KL, White CJ, Haigh ID, Hemer MA, Hoeke RK, Holbrook NJ, Kiem AS, Oliver ECJ, Ranasinghe R, Walsh KJE, Westra S, Cox R (2016) Natural hazards in Australia: sea level and coastal extremes. Clim Change 139(1):69–83. https://doi.org/10.1007/s10584-016-1647-8

McIntosh PC, Church JA, Miles ER, Ridgway K, Spillman CM (2015) Seasonal coastal sea level prediction using a dynamical model. Geophys Res Lett 42(16):6747–6753. https://doi.org/10.1002/2015GL065091

Moftakhari HR, AghaKouchak A, Sanders BF, Matthew RA (2017) Cumulative hazard: the case of nuisance flooding. Earth's Future 5(2):214–223. https://doi.org/10.1002/2016EF000494

Mortensen E, Tiggeloven T, Haer T, Bemmel B, Le Bars D, Muis S, Eilander D, Sperna Weiland F, Bouwman A, Ligtvoet W, Ward PJ (2024) The potential of global coastal flood risk reduction using various DRR measures. Nat Hazard 24(4):1381–1400. https://doi.org/10.5194/nhess-24-1381-2024

Mortlock TR, Metters D, Soderholm J, Maher J, Lee SB, Boughton G, Stewart N, Zavadil E, Goodwin ID (2018) Extreme water levels, waves and coastal impacts during a severe tropical cyclone in northeastern Australia: a case study for cross-sector data sharing. Nat Hazard 18(9):2603–2623. https://doi.org/10.5194/nhess-18-2603-2018

Muis S, Haigh ID, Guimarães Nobre G, Aerts JCJH, Ward PJ (2018) Influence of El Niño-Southern oscillation on global coastal flooding. Earth's Future 6(9):1311–1322. https://doi.org/10.1029/2018EF000909

Neal R, Dankers R, Saulter A, Lane A, Millard J, Robbins G, Price D (2018) Use of probabilistic medium- to long-range weather-pattern forecasts for identifying periods with an increased likelihood of coastal flooding around the uk. Meteorol Appl 25(4):534–547. https://doi.org/10.1002/met.1719

Needham HF, Keim BD, Sathiaraj D (2015) A review of tropical cyclone-generated storm surges: Global data sources, observations, and impacts. Rev Geophys 53(2):545–591. https://doi.org/10.1002/2014RG000477

NOAA Operational Oceanographic Products, C., (U.S.), S., Coastal Management., U.S.O., Marine, U., Research., A., Chapel Hill. Renaissance Computing Institute, U, Chapel Hill. Coastal Resilience Center., U., Group., R.P.S., Ocean Associates, I, Consolidated Safety Systems, I, Keeney, A, Dusek, G, Callahan, J, Ratcliff, J, Jima, T, Brooks, W, Marcy, D, Blanton B, Tilson J, Asher TG, Leuttich RA, Widlansky MJ, Rose L, Morse, C, Haddad, J, Waring B (2025) NOAA's Coastal Ocean Reanalysis: Gulf of Mexico, Atlantic, and Caribbean. https://doi.org/10.25923/5ypp-4e84

Palmer K, Watson CS, Power HE, Hunter JR (2024) Quantifying the mean sea level, tide, and surge contributions to changing coastal high water levels. J Geophys Res Oceans 129(8):e2023JC020737. https://doi.org/10.1029/2023JC020737

Parker BB (2007) Tidal analysis and prediction. https://test.repository.oceanbestpractices.org/handle/11329/632

Paulik R, Stephens S, Wild A, Wadhwa S, Bell RG (2021) Cumulative building exposure to extreme sea level flooding in coastal urban areas. Int J Disaster Risk Reduct 66:102612. https://doi.org/10.1016/j.ijdrr.2021.102612

Rasmussen DJ, Kulp S, Kopp RE, Oppenheimer M, Strauss BH (2022) Popular extreme sea level metrics can better communicate impacts. Clim Change 170(3):30. https://doi.org/10.1007/s10584-021-03288-6

Ray RD, Merrifield MA (2019) The semiannual and 4.4-year modulations of extreme high tides. J Geophys Res Oceans 124(8):5907–5922. https://doi.org/10.1029/2019JC015061

Richet O, Holmes R, Chittleborough J, Spillman C, Smith G (2024) What makes a good tide prediction? Application to the Australian coastline. Journal of Operational Oceanography. In review

Rose L, Widlansky MJ, Feng X, Thompson P, Asher TG, Dusek G, Blanton B, Luettich RA, Callahan J, Brooks W, Keeney A, Haddad J, Sweet W, Genz A, Hovenga P, Marra J, Tilson J (2024) Assessment of water levels from 43 years of NOAA's Coastal Ocean Reanalysis (CORA) for the Gulf of Mexico and East Coasts. Front Mar Sci. https://doi.org/10.3389/fmars.2024.1381228

Speer PE, Aubrey DG (1985) A study of non-linear tidal propagation in shallow inlet/estuarine systems part ii: theory. Estuar Coast Shelf Sci 21(2):207–224. https://doi.org/10.1016/0272-7714(85)90097-6

Stephens SA, Bell RG, Ramsay D, Goodhue N (2014) High-water alerts from coinciding high astronomical tide and high mean sea level anomaly in the Pacific islands region. J Atmos Oceanic Tech 31(12):2829–2843. https://doi.org/10.1175/JTECH-D-14-00027.1

Sweet et al (2018) Patterns and projections of high tide flooding along the U.S. coastline using a common impact threshold. NOAA technical report NOS CO-OPS ; 086. https://doi.org/10.7289/V5/TR-NOS-COOPS-086

Sweet WV, Park J (2014) From the extreme to the mean: acceleration and tipping points of coastal inundation from sea level rise. Earth's Future 2(12):579–600. https://doi.org/10.1002/2014EF000272

Sweet WV, Genz AS, Menendez M, Marra JJ, Obeysekera J (2024) Implications of variability and trends in coastal extreme water levels. Geophys Res Lett 51(14):e2024GL108864. https://doi.org/10.1029/2024GL108864

Taylor A, Brassington GB (2017) Sea level forecasts aggregated from established operational systems. J Mar Sci Eng. https://doi.org/10.3390/jmse5030033

Thompson PR, Widlansky MJ, Hamlington BD, Merrifield MA, Marra JJ, Mitchum GT, Sweet W (2021) Rapid increases and extreme months in projections of United States high-tide flooding. Nat Clim Chang 11(7):584–590. https://doi.org/10.1038/s41558-021-01077-8

Vandenberg-Rodes A, Moftakhari HR, AghaKouchak A, Shahbaba B, Sanders BF, Matthew RA (2016) Projecting nuisance flooding in a warming climate using generalized linear models and gaussian processes. J Geophys Res Oceans 121(11):8008–8020. https://doi.org/10.1002/2016JC012084

Wang J, Church JA, Zhang X, Chen X (2021) Reconciling global mean and regional sea level change in projections and observations. Nat Commun 12(1):990. https://doi.org/10.1038/s41467-021-21265-6

Wedd R, Alves O, Burgh-Day C, Down C, Griffiths M, Hendon HH, Hudson D, Li S, Lim E-P, Marshall AG et al (2022) ACCESS-S2: the upgraded Bureau of Meteorology multi-week to seasonal prediction system. J South Hemisph Earth Syst Sci 72(3):218–242. https://doi.org/10.1071/ES22026

Widlansky MJ, Timmermann A, McGregor S, Stuecker MF, Cai W (2014) An interhemispheric tropical sea level seesaw due to El Niño Taimasa. J Clim 27(3):1070–1081. https://doi.org/10.1175/JCLI-D-13-00276.1

Widlansky MJ, Marra JJ, Chowdhury MR, Stephens SA, Miles ER, Fauchereau N, Spillman CM, Smith G, Beard G, Wells J (2017) Multimodel ensemble sea level forecasts for tropical Pacific islands. J Appl Meteorol Climatol 56(4):849–862. https://doi.org/10.1175/JAMC-D-16-0284.1

Woodworth PL, Melet A, Marcos M, Ray RD, Wöppelmann G, Sasaki YN, Cirano M, Hibbert A, Huthnance JM, Monserrat S, Merrifield MA (2019) Forcing factors affecting sea level changes at the coast. Surv Geophys 40(6):1351–1397. https://doi.org/10.1007/s10712-019-09531-1